

A BER-Based Partitioned Model for a 2.4 GHz Vehicle-to-Vehicle Expressway Channel

GUILLERMO ACOSTA-MARUM and MARY ANN INGRAM

*School of Electrical and Computer Engineering, Georgia Institute of Technology, Atlanta, GA 30332-0250, USA,
E-mails: gacosta@gatech.edu, mai@ece.gatech.edu*

Abstract. Statistical channel models based on BER performance are presented for a frequency- and time-selective vehicle-to-vehicle wireless communications link in an expressway environment in Atlanta, Georgia, where both vehicles traveled in the same direction. The models are developed from measurements taken using the direct sequence spread spectrum (DSSS) technique at 2.45 GHz. A collection of tapped delay line models, referred to as a “partitioned” model in the paper, is developed to attempt to capture the extremes of BER performance of the recorded channel. Overall and partition models are compared to the recorded channel in terms of the BER statistics obtained when the channels are inserted in a dedicated short range radio (DSRC) standard simulation system. The quality of the match between synthesized and recorded channel BER statistics is analyzed with respect to type of modulation (fixed or adaptive), the frame length, and the length of the interval over which the BER was calculated.

Keywords: high mobility channel, frequency-selective, DSRC, wideband RF channel modeling, time-selective, large-scale fading, dynamic model

1. Introduction

With increasing interest in mobile ad hoc networks (MANETs) [1], comes the need to more carefully model the mobile-to-mobile wireless channel. MANET applications include battle-ground communications [2], mobile sensor networks [3, 4], and Intelligent Transportation Services [6]. For the latter application, the dedicated short range radio (DSRC) standard (802.11p) [7] has been developed. Such channels are also of interest in cooperative diversity or fading relay channels [5]. The wideband vehicle-to-vehicle (VTV) channel is “doubly selective;” this means that its frequency response varies significantly over the signal bandwidth and its time fluctuations happen in the course of a symbol period. The small-scale fading characteristics of such a channel are typically modeled by a tapped delay-line with time-varying, but stationary tap gains that are described by their K -factors and power spectral densities (“spectra”). Like other wireless channels, the VTV channel undergoes both small-scale and large-scale random fluctuations, and characterization of both types is important for reliable system design. In the VTV channel, the large-scale fluctuations are manifested by changes in the tap delays, relative tap powers, tap K -factors, and shapes of the tap spectra. It is the aim of this paper to identify these changes using a bit error rate (BER)-based approach for the expressway channel, at 2.4 GHz, when both vehicles travel in the same direction.

Other authors have proposed stochastic propagation models that capture both small- and large-scale random fluctuations [8–11]; these types of models are sometimes called “dynamic models” [8–10]. For the indoor frequency selective channel, Nielson et al. [9] represent the power delay profile (PDP) as a superposition of path clusters. The large-scale

random fluctuations are modeled by letting the value of the PDP for each bin change over time according to an autoregressive random process. The other authors [8, 10, 11] associate with each path or delay a random time of “birth” when the path first appears, and a random time of “death” when it disappears. Newton et al. [10] used a modified Poisson process to determine which PDP bins are occupied, and empirically based distributions to model path strengths and lifetimes. The authors of [8] and [11] employ actual birth-death (BD) Markov models to govern existences of paths. In all of these works, sequences of short-term or small-scale fading models (PDPs or PDPs plus angle-of-arrival profiles) were first identified. Next the large-scale models such as BD processes were identified from the fluctuations of the model parameters across the sequence. Finally, the resulting dynamic model was evaluated by comparing key features of the recorded and simulated channels, such as BD probability matrix [8] or cumulative distribution functions (CDFs) of delays and angular spreads [11].

The present work shares the first step with the previous approaches, but takes a different, BER-based approach to modeling the large-scale fluctuations.

The approach of this paper is based on the premise that the simulated channel should produce BER statistics that are similar to selected measured channels. Preliminary models with stationary tap gains failed to match the wide variation in BERs produced by the recorded expressway channel. This result motivated the work that is reported in this paper, which is an investigation into the design of a small collection of doubly selective models, such that when simulated in succession, produce long-term BER statistics that are similar to those of the measured expressway channel.

Other related works include theoretical 2-D [13] and 3-D [14] VTV models, flat-fading VTV measurements for the highway [15], and doubly selective models for the roadside-to-vehicle channel [16]. Some examples of long and short term tap spectra for the VTV channel were presented by the authors in [17]; to the authors’ best knowledge, these were the first reported VTV measured tap spectra. In this paper, the same expressway measurements reported in [17] are used to identify the collection of doubly selective models.

In the following section, we describe why we chose the expressway site and how we performed the channel sounding campaign. In the next section, we present the methodology used to obtain a statistical model from the recorded data. In Section 4, we show our first model approach and the evaluation tools. In Section 5, we present the partitioned models. In Section 6, we have the model performance results as compared to the real recorded channel. Finally, we present conclusions in the last section.

2. Measurement Procedure

The VTV channel sounding campaign consisted of two phases. In the first phase, we looked for sites with long delay spreads, and in the second phase, we performed a detailed channel sounding in the sites with the largest delays.

2.1. SITE SELECTION PROCEDURE

To obtain the results in this paper, a VTV delay profile survey was first conducted in the Atlanta, Georgia metropolitan area, using an off-the-shelf 802.11b channel “sniffer.” The sniffer provided impulse responses (IRs) with 22 bins each 50 ns wide, power level, and

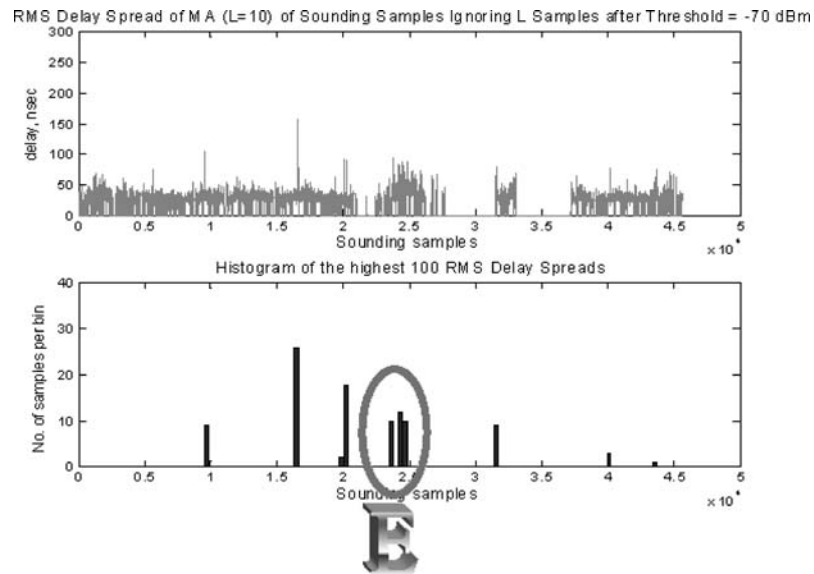


Figure 1. Above threshold RMS delay spread MA with corresponding histogram.

GPS coordinates. The device used the 11 symbol Barker code as a sounding signal, but since its transmission timing depends on the frame request, there is no way to know the repetition rate. We performed four sessions of measurements where we covered areas that we considered typical of urban environments such as expressways, tunnels, under and over passes, urban canyons, etc. For each session, we processed the data by setting four power level thresholds: -90 , -80 , -70 , and -60 dBm. For each threshold, we specified the location of all the samples below it. Not all the sample sets allowed the four threshold levels. We then obtained the RMS delay spread for each of the available impulse responses. We then performed a moving average (MA) of length $L = 10$ of these RMS values, where we ignored the samples located below the threshold and the following L . For each set of averaged samples, we obtained a histogram of the times of the 100 highest values. We obtained a total of 20 sets. We then selected the times where the histograms indicated a significant cluster independent of the threshold level; i.e., where the cluster repeated for different power thresholds. Since each sample set had GPS information, we could locate these clusters. With the clusters' geographical coordinates, we were able to obtain aerial photos of the locations. Once we looked at these photos, we could explain the clusters. These aerial photos are centered at the GPS coordinates. We present the cluster for the expressway in Figure 1 and its corresponding aerial photograph in Figure 2.

Later, measurements of the joint delay-Doppler characteristics were performed at the selected sites using a custom channel sounder that used the direct sequence spread spectrum (DSSS) technique [18].

In this paper, we present the results obtained in the expressway. During the measurements, the vehicles traveled with the traffic flow: precise position of the vehicles was not available, and sometimes intervening vehicles blocked the line-of-sight (LOS). The measurement vehicles were traveling in the same direction, from right to left in the figure (westbound), at a speed of about 55 mph in the slow lane. The freeway had a wall about five feet high dividing the eastbound lanes from the westbound lanes.



Figure 2. Location E (33.9179, -84.3392), an expressway intersection with nearby office buildings.

2.2. HARDWARE SETUP

The channel was measured using the spread spectrum approach described in [3]. As shown on the right in Figure 3, an Agilent™ ESG4438C RF signal generator was used to create the maximum length sequence waveform of 511 chips, with the chip period of 50 ns, and a 3 dB bandwidth of approximately 20 MHz, centered at 2.445 GHz. The 511-chip burst was repeated back-to-back, corresponding to a repetition period of 25.5 μ s, which further corresponds to a maximum unambiguous excess path length of 7.65 km and a maximum unambiguous Doppler shift of 19.5 kHz. Following amplification and transmission from a 8 dBi omnidirectional antenna mounted on the middle of the roof of a compact car, the signal power was 2.1 W (ERP), which enabled measurements over ranges of up to 300 m.

The receiver front end, shown on the left in Figure 3, consisted of another 8 dBi omnidirectional antenna, mounted on the middle of the roof of a van, followed by a HyperAmp™ HA2401DX-AGC100 low noise amplifier and a custom down-conversion to a first IF of 445 MHz, and then to a second IF of 20 MHz. The first IF filter 3 dB bandwidth was approximately 46 MHz. The backend of the receiver begins with the A-to-D converter in the Pentek 6235, sampling with 12 bits at 80 MHz. The recorded channel is sampled every $\Delta\tau = 1/B = 50$ ns, where B is the measurement real baseband bandwidth of 20 MHz. The samples are fed to the digital downconverter also in the Pentek 6235, which included a 10 MHz output lowpass filter. As we will explain later, there was a miss-match between this output filter bandwidth and the signal's bandwidth. The complex baseband samples were transferred via an FPDP link at a rate of 20 Msamples/s and were recorded directly into a hard disk array at 80 Mbytes/s. Prior to a recording session, the transmitter clock and the master receiver clock were synchronized to within a few Hz. Testing under various conditions confirmed that the clock offsets remained at these low levels.

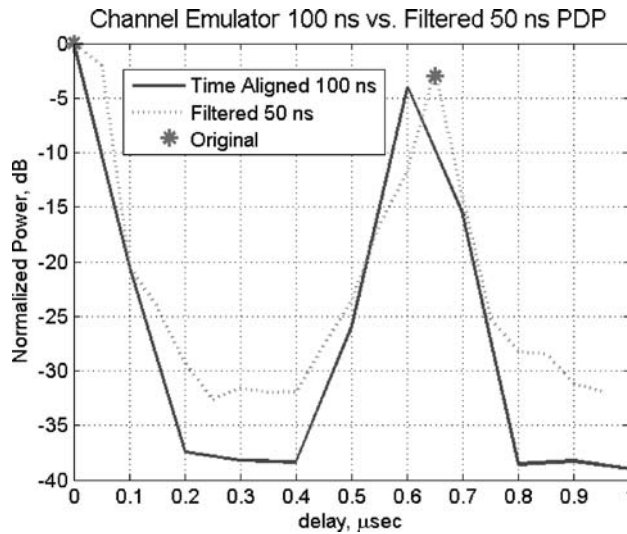


Figure 5. 50 ns and 100 ns system testing using a channel emulator.

2.4. MEASUREMENT SYSTEM TESTING

To verify the system's performance, we performed an experiment using a channel emulator. We emulated a two-tap channel with delays at 0 and 650 ns and with powers of 0.0 and -3.0 dB respectively. In Figure 5, we show the performance of the system as we used it to record the data compared to what the performance should be according to system's specifications. As described in Section 2.2, the maximum recording speed of the system is 20 Mega-complex samples per second, which correspond to a complex baseband bandwidth of ± 10 MHz. For this bandwidth, the maximum attainable resolution is 100 ns. If we sample with 100 ns period, our PDP peaks occur only at multiples of 100 ns. We notice that with 50 ns sampling there is a loss of dynamic range, but there is a much better tap resolution. We also notice that because of the 10 MHz lowpass filter, we have correlated fading as we can see in the filtered response at 50 ns. This experiment was repeated for different delays and powers, with similar results. We elected to use 50 ns sampling so we could have the higher resolution.

3. Model Development

In this section, we describe the statistical procedure to obtain the parameters. We first describe how we obtained the tap delay line models to capture small-scale fading characteristics. Next, we explain two approaches to capturing large scale fluctuations. Finally, we evaluate the models by comparing the simulated and recorded channels in terms of BER statistics.

3.1. INITIAL TAP CHARACTERIZATION

In this paper, we compare several modeling approaches, but they all start with estimation of the tap parameters of power and delay from a given record of measured data. This first modeling stage is intended to capture small-scale fading. The modeling approaches differ in the length of the record.

The first step in extracting the model is to separate the fast from the slow fading characteristics. We can obtain the slow fading by obtaining the local average power [17]. For this, we require uncorrelated samples of the IR over an appropriate distance that will average out the short-term fading and will not smooth out the long-term fading. This length is usually in the range of 20 to 40 wavelengths, and a sampling at 0.8 of the wavelength is usually enough to achieve uncorrelated samples. We calculate the PDP by averaging the magnitude squared of the IR

$$P(n\Delta\tau) = \frac{1}{Q} \sum_{k=0}^{Q-1} |h_{\text{norm}}(n\Delta\tau, k\Delta t)|^2 \quad 0 \leq n \leq N - 1, \quad (1)$$

where $k\Delta t$ is the fixed observation instant of the k -th single IR, Q is the total number of IRs, and h_{norm} indicates short-term fading only. Next, we determine the significant part of the PDP by discarding all parts that are more than 30 dB down from the strongest path.

For the expressway location, we recorded 14 ten-second takes. As mentioned before, we divided each take into 12 0.7-second segments for their analysis. Please note that each take corresponds to a physically different time and location, i.e., each take could be minutes and kilometers apart from another. In Figure 6, we show the PDPs computed for all the 0.7 s segments of the 14 takes. We observe that most of the PDPs die out before $1 \mu\text{s}$, because of the generally confined nature of the channel.

Let L be the length of the significant part of the PDP divided by $\Delta\tau$. Let M be the number of taps in the model, such that $M < L$. The L samples are divided into M groups. If the result $L/M = I$ is not an integer, samples with zero amplitude are added to the end of the PDP. The tapped delay value in each group is found by [2]

$$\tau_m = \frac{\sum_{n=i_m}^{i_m+I-1} n\Delta\tau \cdot P(n\Delta\tau)}{\sum_{n=i_m}^{i_m+I-1} P(n\Delta\tau)} \quad \text{for } 0 \leq m \leq M - 1, \quad (2)$$

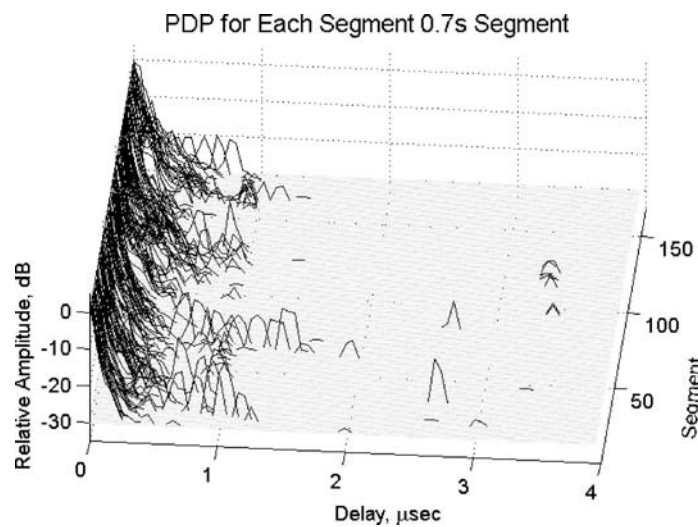


Figure 6. Expressway PDPs.

where i_m is the sample number at the start of each group. The delay of the first tap is $\tau_0 = 0$. Knowing the delay position of the tap, we can obtain the tap magnitude as follows:

$$P_m(\tau_m, k\Delta t) = \frac{1}{I} \sum_{n=i_m}^{i_m+I-1} P(n\Delta\tau). \quad (3)$$

To obtain the Doppler spectra for each model tap, we first use the Welch algorithm to estimate the Doppler spectrum for each of the significant bins or bins above threshold obtained from the PDP. We then use the same interval I to average the spectra across the bins in the interval.

4. Modeling the Large-Scale Fluctuations

4.1. OVERALL MODELS

At first, we did not attempt to model the large-scale fluctuations. We considered that since most commercial channel emulators are six or 12 taps per channel, it would be a good idea to generate six and 12-tap channel models. First, we generated a model for each of the 0.7 s segments, and then, we generated overall models by averaging the parameters of all the segment models. When we averaged the parameters, we encountered a problem in the averaged tap delay values since they were not monotonically increasing. As we can see in Figure 6, many of the significant bins of each segment PDP will not be consecutive. In particular for the latter taps, the average will include many zeros and decrease the final delay value. We tried either artificially considering all the bins as consecutive or ignoring the zero elements in the average. Neither of these produced an increasing delay value. Another problem with this approach was that the averaged spectra included contributions from quite different delays, which created excessively wide spectra. The excessively wide spectra caused very high BERs, and because of this, we rejected this approach.

To solve the delay position inconsistencies, we decided to regenerate the overall model considering just one PDP for the complete data set. We achieved the latter by setting $Q = (14 \times 12 \times 27400)$ in (1). This complete PDP contained only 10 significant bins, which happen to be consecutive. We then followed the previously described methodology to generate the model described in Table 1. In this table, we specified the number of taps, the tap delay, the tap power magnitude, and the K-factor. We will further discuss this K-factor in a later section. From these statistical parameters we obtain the model whose scattering function we present in Figure 7.

The first thing we notice in the Doppler spectra is the “LOS-like” or Rician behavior for each of the first paths. This suggests that there are many reflectors traveling at a similar speed to the terminals. We also notice a widening of the Doppler spectra for the later taps. This widening is in accordance to the flat fading results of [15]. In several of these later spectra, we can notice some small spikes on the sides of the spectra. The frequencies of these spikes are approximately equal to the maximum and minimum Doppler shifts of single-bounce paths; therefore, we conclude that they were caused by the transient paths reflecting from highway overpasses.

From Figures 8 and 9, we can also notice that for such a high K-factor, the peak of the first tap spectrum looks “wide.” We can deduce that there are two factors contributing the tap spectrum widening. The first factor is the difference in frequency shift for each of the data

Table 1. Overall 10-Tap model parameters.

Tap	Delay, ns	Relative power, dB	K_{Rice}
1	0	0.0	102.0
2	50	-6.5	7.3
3	100	-14.4	4.7
4	150	-17.5	3.6
5	200	-19.7	1.8
6	250	-22.0	0.5
7	300	-24.4	0.2
8	350	-25.3	0.2
9	400	-27.1	0.0
10	450	-28.1	0.0

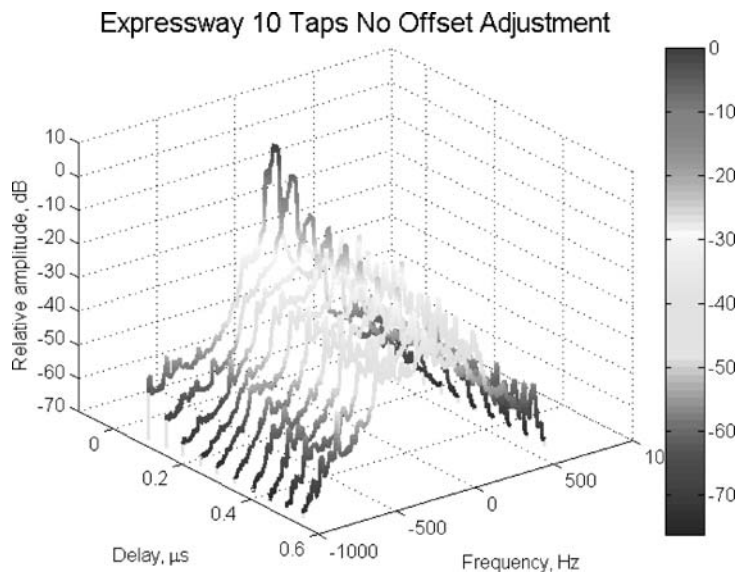


Figure 7. Scattering function for the overall 10-tap model without frequency adjustment.

segments. This effect is better seen in the first bin where we have the LOS. The general shape for this bin spectrum is a high narrow peak with a lower wide base. The frequency position of this narrow peak varies from segment to segment since the vehicles positions are different. When we average the contributing spectra, the different peak positions will cause a broad central peak as seen in Figure 8. The other effect is the averaging by itself. As indicated by the thick line, the averages tend toward the wider section of the spectra set.

We can reduce the widening caused by the different frequency offsets by centering each of the spectra before averaging. To do so, we need to estimate the offset separately for each of the bins and shift each of them independently. We obtained the offset value by treating the spectra as a probability distribution and obtaining its first moment after normalization. In Table 2, we have the correlation coefficients of the frequency offsets where we can conclude that there is no one single frequency shift measure that can be applied to all the taps.

Table 2. Spectra offset correlation coefficient matrix.

1.00	0.83	0.59	0.52	0.45	0.39	0.30	0.21	0.25	0.31
0.83	1.00	0.82	0.58	0.50	0.37	0.24	0.12	0.18	0.24
0.59	0.82	1.00	0.66	0.46	0.29	0.10	-0.01	0.07	0.15
0.52	0.58	0.66	1.00	0.71	0.42	0.22	0.08	0.12	0.24
0.45	0.50	0.46	0.71	1.00	0.73	0.41	0.18	0.20	0.12
0.39	0.37	0.29	0.42	0.73	1.00	0.75	0.44	0.39	0.14
0.30	0.24	0.10	0.22	0.41	0.75	1.00	0.75	0.53	0.28
0.21	0.12	-0.01	0.08	0.18	0.44	0.75	1.00	0.71	0.34
0.25	0.18	0.07	0.12	0.20	0.39	0.53	0.71	1.00	0.66
0.31	0.24	0.15	0.24	0.12	0.14	0.28	0.34	0.66	1.00

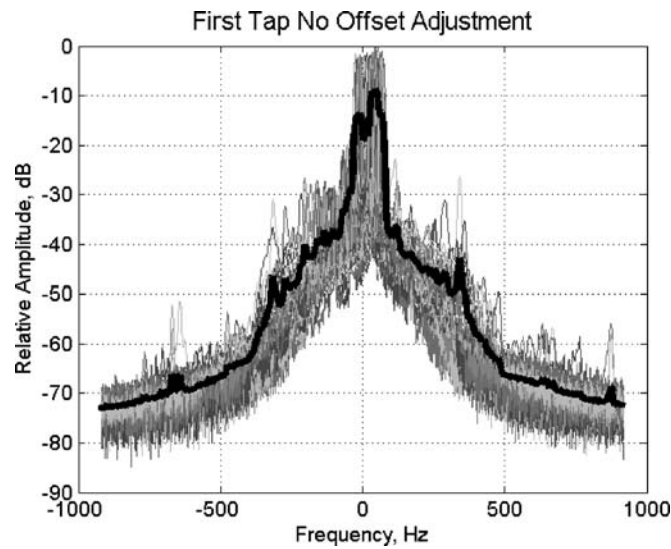


Figure 8. All the spectra contributing for the first tap of the overall model. The thick line represents the tap spectrum.

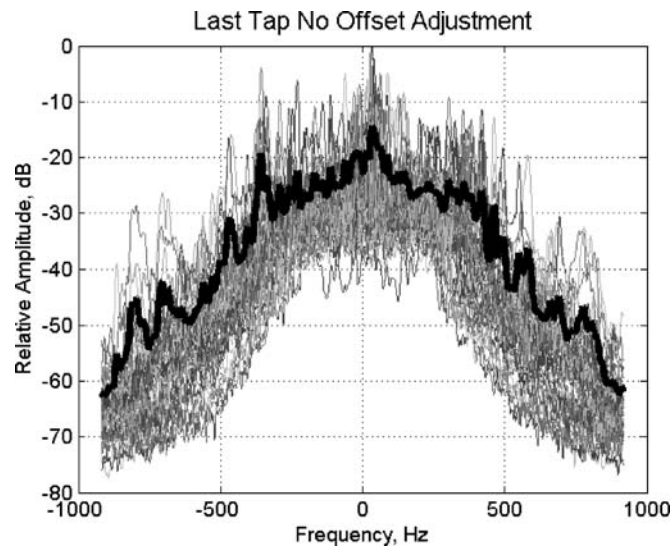


Figure 9. All the spectra contributing for the last tap of the overall model. The thick line represents the tap spectrum.

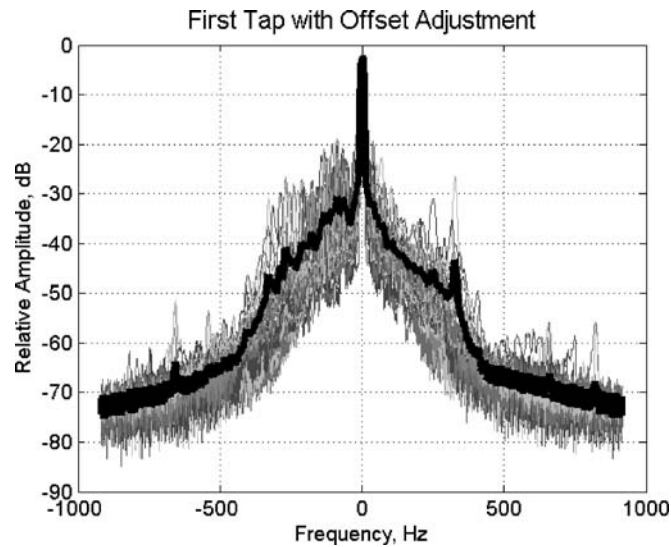


Figure 10. Frequency aligned spectra contribution for the last tap of the overall model. The thick line represents the tap spectrum.

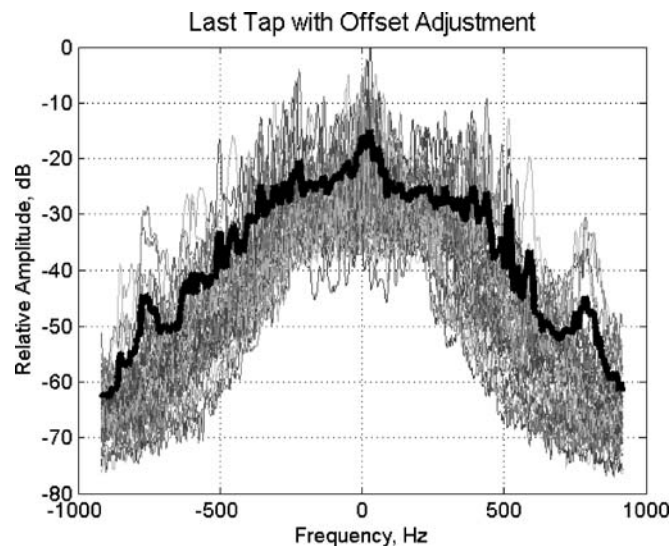


Figure 11. Frequency aligned spectra contribution for the last tap of the overall model. The thick line represents the tap spectrum.

In the next two figures, Figures 10 and 11, we show the improvement obtained after the frequency offset adjustment. We now have a narrow peak in the first tap as wanted. We still have the widening effect of the averaging, but it is reduced. In Figure 12, we have the corresponding scattering function for the frequency adjusted model.

4.2. DSRC SIMULINK™ MODEL FOR CALCULATING BER

The primary means of model evaluation is the BER distribution derived from simulations of the DSRC standard [7]. Samples of BER are calculated from non-overlapping time windows. The

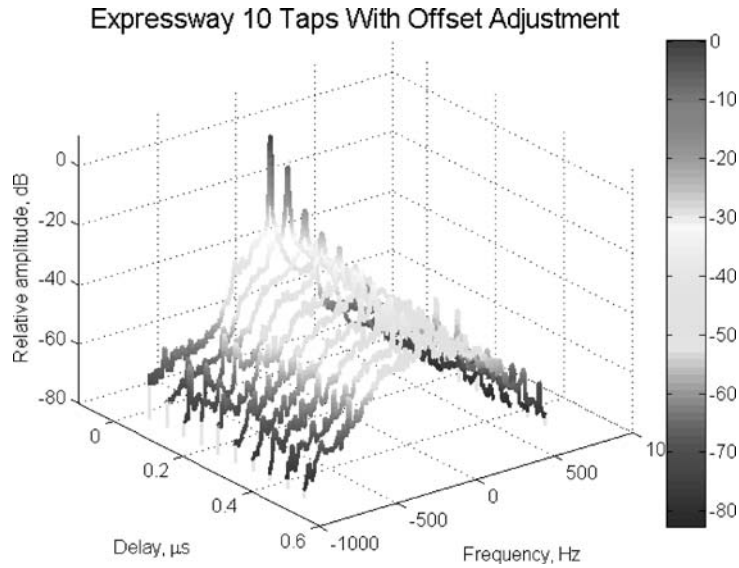


Figure 12. Overall 10-tap model with frequency adjustment scattering function.

differences of BER from different time windows reveal the dynamics or large-scale fluctuations of the channel. Since BER simulation is the primary evaluation tool, it is described in this section.

As part of our model development approach, we compared the BER performance of a DSRC link over the recorded channel and over the synthesized channels. We normalized all the channels so that their PDPs had unit area; this includes separate normalization for each measured segment. We developed a SimulinkTM model that follows faithfully the specifications of the DSRC standard [7] shown in Table 3. The model includes all the transmission modes and coding. The channel insertion works by using each IR as a FIR filter coefficients set. We designed the receiver to include channel adaptive equalization using the pilot tones following the specifications in [23]. The model also contains a signal-to-noise ratio (SNR) threshold detector to adaptively change among the eight transmission modes. The noise is defined as the mean square of the difference between the received complex symbol and its corresponding constellation point. Both the adaptive equalizer and adaptive modulator operate on a frame by frame basis. For the simulations we choose a frame size of 64 OFDM symbols. We believe that this frame length allows the system to cover all the modulation modes. The OFDM symbol is modulated in only 52 subcarriers out of 64 and has $8.0 \mu\text{s}$ duration with a $1.6 \mu\text{s}$ guard band interval. The total occupied bandwidth is 8.3 MHz. No thermal noise was added in our simulations.

4.3. CHANNEL SYNTHESIS

To measure BER, we need first to synthesize the channel by producing IRs according to the statistical channel parameters. Then we need to insert this channel into a simulation system, which we just described. To synthesize the channel, we use filtered noise on each tap, where the filter characteristics match the spectra of the statistical model [22]. As an example, we show in Figure 13 the short-term Doppler spectra and the long-term Doppler spectrum of

Table 3. DSRC standard specifications [7].

Data rate, mbps	Modulation	Coding rate	Coded bits per OFDM symbol	SNR Threshold dB
3	BPSK	1/2	48	<10
4.5	BPSK	3/4	48	10
6	QPSK	1/2	96	11
9	QPSK	3/4	96	14
12	16-QAM	1/2	192	18
18	16-QAM	3/4	192	22
24	64-QAM	2/3	288	26
27	64-QAM	3/4	288	28

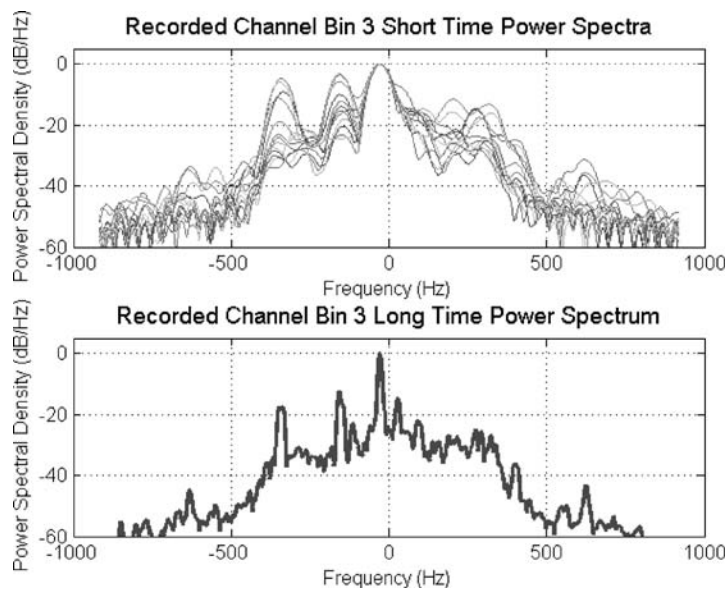


Figure 13. Short time Doppler spectra (50 ms) and long time Doppler spectrum (0.7 s) for bin three of one recorded 0.7 s segment.

the third bin of a randomly selected recorded 0.7 segment. For the long-time spectrum, we used the approximately 27,400 IRs in 0.7 s for the estimate, and for the short-time spectra, we obtained the estimate every 2,048 IRs or approximately every 50 ms. In Figure 14, we do the same for also a randomly selected synthesized 0.7 s segment. As we can see in these figures, the short-time spectra of the synthesized channel have transient behavior similar to that of the real channel.

5. Partitioned Model

In this section, we present two other approaches for modeling the VTV channel. As we will show in the Results section, the two overall channels do not provide the same extremes of performance that the recorded channel provides. After analyzing the behavior of the recorded channel, we observed that there are two correlated parameters with a wide range of variation:

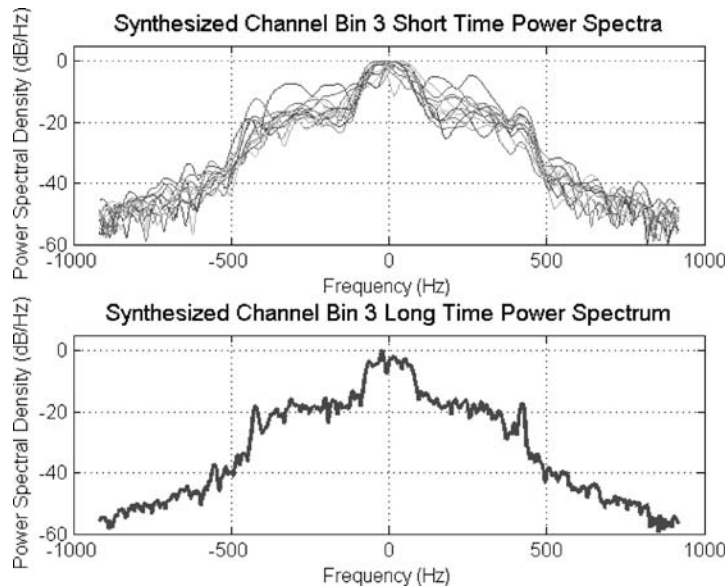


Figure 14. Short time Doppler spectra (50 ms) and long time Doppler spectrum (0.7 s) for bin three of one synthesized 0.7 s segment.

BER and maximum delay. We decided to use these parameters to partition the recorded channel data into sets with similar BER performance or similar delay profile characteristics. We need to emphasize that we performed frequency offset alignment in both models.

5.1. BER PARTITIONS

For the partition with respect to BER performance, we divided the recorded 0.7 segments according to their BER after simulation with a 64 symbol frame and adaptive modulation. We define four partitions for each order of magnitude of the BER starting at 10^{-4} as shown in Table 4. In this table, we indicate the number of segments belonging to each partition along with the number of taps used in the partition's statistical model. We also show the average BER for each partition for the corresponding recorded channel segments and for the synthesized channel derived from each partition model. It is interesting to notice that the synthesized channel BER stays in the same order of magnitude, which makes it higher for two partitions and lower for two. We do not have a concrete explanation for this behavior, but we think that the fixed number of taps for every synthesized IR reduces the BER variability from segment to segment.

We show the scattering functions for the first and fourth partitions in Figure 15 and Figure 16 respectively. From these figures, we can observe that the higher BER partition has longer delays and wider spectra.

5.2. MAXIMUM DELAY PARTITION

For the maximum delay partition model, we create the partitions according to the number and position of the significant bins of each 0.7 s PDP. First we identified the PDPs with consecutive significant bins. We found from five and up to 12 consecutive significant bins after the first.

Table 4. Partition by BER criterion results.

BER Partition	Selection criterion: BER per 0.7 s segment	Number of 0.7 s segments	Partition recorded channel average BER	Number of taps in partition statistical model	Partition synthesized channel average BER
1	$BER \leq 10^{-4}$	11	7.407×10^{-5}	4	1.668×10^{-3}
2	$10^{-4} < BER \leq 10^{-3}$	55	4.066×10^{-4}	4	2.419×10^{-3}
3	$10^{-3} < BER \leq 10^{-2}$	87	3.862×10^{-3}	5	2.881×10^{-3}
4	$10^{-2} < BER \leq 10^{-1}$	15	1.656×10^{-2}	7	8.344×10^{-3}

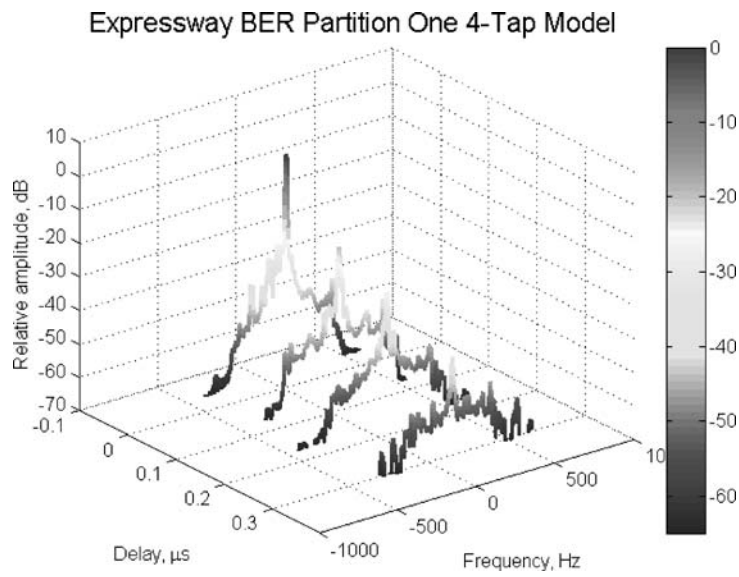


Figure 15. BER partition one scattering function.

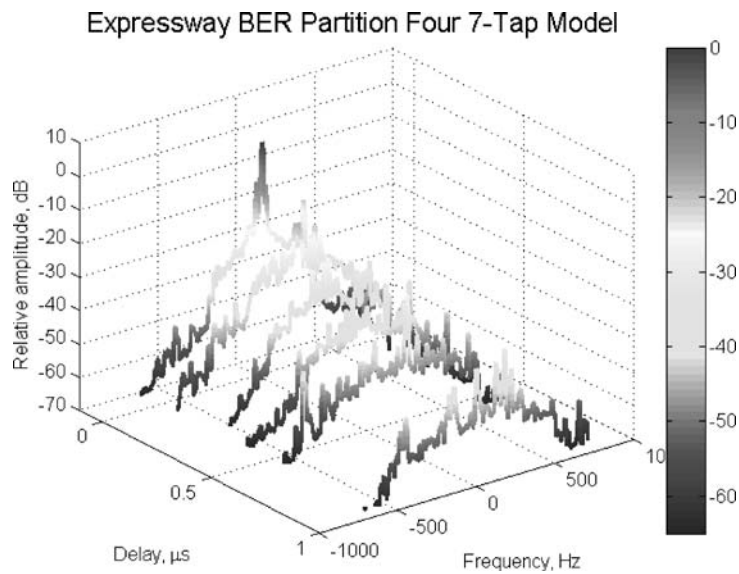


Figure 16. BER partition four scattering function.

Table 5. Partition by maximum criterion results.

Maximum delay partition	Selection criterion: BER per 0.7 s segment	Number of 0.7 s segments	Partition recorded channel average BER	Number of taps in partition statistical model	Partition synthesized channel average BER
1	5 & 6 Consecutive first significant bins	24	6.679×10^{-4}	3	2.639×10^{-3}
2	7 & 8 Consecutive first significant bins	31	1.060×10^{-3}	4	3.049×10^{-3}
3	9 & 10 Consecutive first significant bins	12	1.188×10^{-3}	5	2.622×10^{-3}
4	11 & 12 Consecutive first significant bins	12	7.537×10^{-3}	6	6.184×10^{-3}
5	Long (>12) Non-consecutive significant bins	65	6.762×10^{-3}	11	4.615×10^{-3}
6	Short (<12) Non-consecutive significant bins	24	1.541×10^{-3}	5	2.465×10^{-3}

From this set, we created four partitions so that each partition model would contain two consecutive bins per tap. For the non-consecutive significant bins, we created two partitions: one for segments with less than 12 significant bins and one for segments with 12 or more significant bins. The number of segments per partitions is shown in Table 5 where we also indicate the number of taps for the partition model. As in the previous table, we also show the BER per partition for recorded and synthesized channels. Once again, we obtained BER of the same order of magnitude for the synthesized channel.

6. Results

In this section, the models developed in the previous sections are compared in terms of the cumulative distribution function (CDF) of the BER. The BER is impacted strongly by the length of the frame, the length of the time period over which the BER is computed, and the choice of fixed or adaptive modulation. Longer frames yield higher BER because the high initial quality of the channel estimates degrades over time, even though there are pilot tones. The shape of the CDF of the BER is impacted by the length of the observation interval because zero and very low values of BER become less likely as the interval grows. Finally, the type of modulation, fixed or adaptive, makes a difference, because ideally, adaptive modulation makes the BER constant.

The BER will be computed for four cases, two which use adaptive modulation and short frames, and two which use fixed modulation (6 Mbps) and long frames. The latter case was included because it is the basis of the motion-related equipment test in the current DSRC standard [7]. For adaptive modulation, two interval lengths are considered: 0.7 s, which corresponds to the “segment” length in the database, and $544 \mu\text{s}$, which corresponds to a frame containing 64 symbols. For fixed modulation, the two interval lengths are 0.7 s and 1.376 ms. The 1.376 ms frame holds 168 symbols, or 1000 bytes of information at 6 Mbps; this is the “long frame” part of the motion-related equipment test in the DSRC standard.

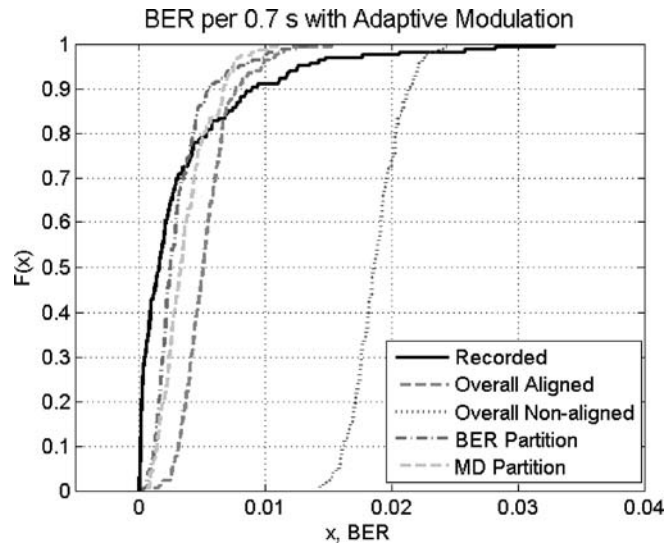


Figure 17. Recorded channel and models CDFs of the BER per 0.7 s segment, a 64 OFDM symbol frame, and adaptive modulation.

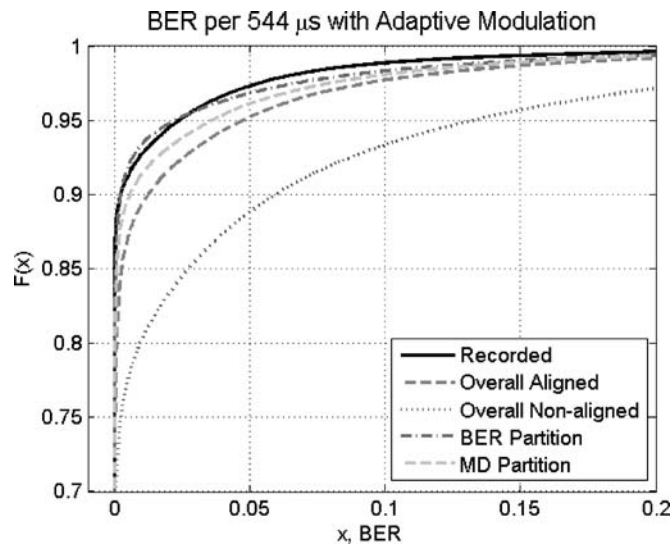


Figure 18. Recorded channel and models CDFs of the BER measured for each 64 OFDM symbol frame and adaptive modulation.

Figures 17 and 18 contain the adaptive modulation results and Figures 19 and 20 contain the fixed modulation results. The adaptive modulation results include CDFs of BER for the recorded channel and four models: the overall aligned, the overall non-aligned, the BER partition, and the maximum delay partition. Recall that for all models except the overall non-aligned model, the segment spectra are centered prior to averaging. The fixed modulation results include only the recorded channel and the BER partition model.

In Figure 17, the recorded channel BER has a larger variance than each of the models. Observation of bit errors versus time (not shown in this paper) indicate that the recorded

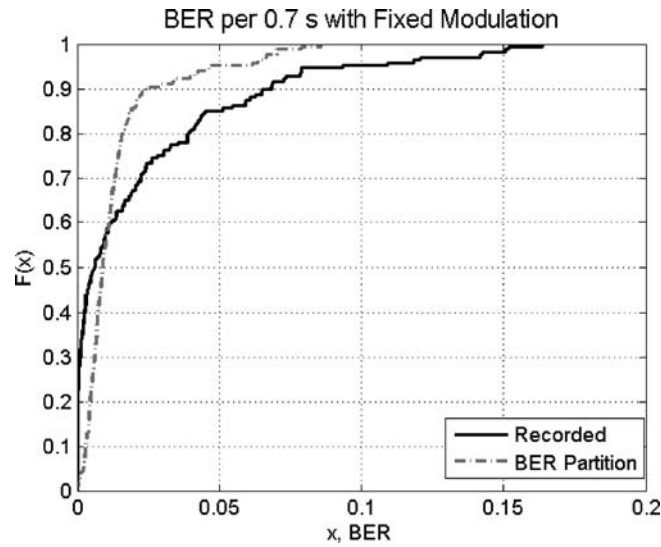


Figure 19. Recorded channel and BER partition model CDFs of the BER per 0.7 s segment, a 168 OFDM symbol frame, and a fixed 6 Mbps modulation.

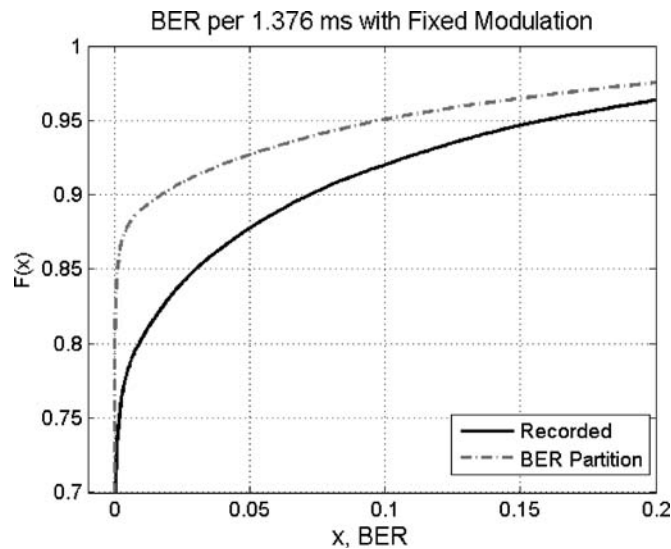


Figure 20. Recorded channel and BER partition model CDFs of the BER measured for each 168 OFDM symbol frame (1000, data bytes) with fixed 6 Mbps modulation.

channel has relatively long periods of time when there are no errors, and then other periods of time with a high density of bit errors. In contrast, the synthesized channels produce a more uniform distribution of errors in time. Because the recorded channel produces a significant percentage of 0.7 segments with zero or very few errors, we may conclude that the low-error periods are often at least 0.7 s long.

In Figure 18, the BER partition model produces a very good fit to the recorded channel. The MD partition model is next closest, and the overall aligned model is the worst fit of the aligned models. Evidently, the 64 symbol frame is short enough that the synthesized models produce between 80 and 90 percent error free frames.

As observed in Figure 19 and Figure 20, the long frames and fixed modulation degrade the performance of the recorded channel and all the models. Interestingly, the BER partition model and recorded channel diverge significantly for in the low BER region when BER is computed over the long frame period (1.376 ms). Comparing Figure 18 and Figure 20, we observe that the BER partition model is only slightly degraded by the longer frame and fixed modulation, but the recorded channel degrades significantly for the longer frame. Long frame vs. short frame effects would seem to depend more on small scale phenomena than large scale, and the long frame would suffer more from Doppler spread. One possible reason for the divergence of these curves is that the design of the partition model was based on the short frame and adaptive modulation, yet in Figure 20, the model is being evaluated on a link using a different type of modulation. Had the partition model been based on the modulation assumed in Figure 20, fewer segments would have been assigned to the lowest BER partition. The excessive number of segments in the low BER partition could be the reason that the BER partition model performs so much better than the recorded channel in the low BER regime.

6.1. K-FACTOR

The Rice or K factor is not part of our model specification (*i.e.* the K-factor is implied by the spectrum), but it is an important feature of models; therefore, it should be examined. Also, K-factors must be explicitly specified in RF channel emulators. For these reasons, in this section, we compute the K-factors of the taps of our models and compare them to the recorded channel. We determine the Rice or K factor for any bin m using the moment-method [20, 21] as follows:

$$\begin{aligned}
 G_k &= |h_m(\tau_m, k\Delta t)|^2, \quad k = 1, \dots, Q \\
 G_a &= \frac{1}{Q} \sum_{k=1}^Q G_k \\
 G_v &= \sqrt{\frac{1}{Q} \sum_{k=1}^Q (G_k - G_a)^2} \\
 |V|^2 &= \sqrt{G_a^2 - G_v^2} \\
 \sigma^2 &= G_a - |V|^2 \\
 K_{\text{Rice}} &= \frac{|V|^2}{\sigma^2}.
 \end{aligned} \tag{4}$$

where $h(\tau_m, k\Delta t)$ is the k th IR with bins at delay τ_m . Applying (4) to each 0.7 s recorded segments, for which $Q = 27,400$, we obtained a 168×511 K-factor matrix. Any complex K-factors were set to zero. The K-factors given for the overall model in Table 1 are the first ten column averages of the K-factor matrix. In Table 6, we present the K-factors for the corresponding rows and columns of the K-factor matrix for each of the sections of the BER partition model. For example, for Partition One; we have 11 0.7 s segments and seven significant bins for the PDP of the partition. To obtain the K-factors for the partition, we choose the corresponding rows and columns, and we perform a column average on the new 11×7 matrix. For Table 6, we also calculated the K-factors for the

Table 6. K-factors for the BER partition model.

Partition one bins	Partition one taps	Partition two bins	Partition two taps	Partition three bins	Partition three taps	Partition four bins	Partition four taps
159.4	0.8	174.8	1.2	61.8	1.1	26.5	1.1
5.1		8.1		7.1		8.0	
13.3	0.4	6.5	0.4	3.1	0.4	1.3	
10.0		6.0		1.8		0.6	0.2
5.9	0.3	3.6	0.2	0.6	0.3	0.7	
1.8		1.1		0.4		0.2	
0.1	0.3	0.4	0.2	0.4	0.2	0.7	0.2
		0.4		0.5		0.1	
				0.1	0.2	0.0	
						0.1	0.2
						0.0	
						0.0	
						0.0	0.2
						0.0	
						0.0	
						0.0	0.3
						0.0	
						0.1	
						0.4	0.3

synthesized channel. Continuing with the partition one example, the partition contains four taps; therefore, the K-factor submatrix size is 11×4 . Each matrix element was obtained from the 27,400 samples per tap of the synthesized channel. The table values are the column averages.

By looking at the scattering function of Figure 15, we would expect a high K-factor for the first tap, but it is surprisingly small. Our only explanation is the widening of the lower part of the tap produced by the averaging. We also notice that the segments with low BER present very high K-factors in the first bin. We believe that the correlation between BER and K-factor should be further investigated.

7. Conclusions

Overall and partitioned models have been investigated for the VTV doubly selective expressway channel at 2.4 GHz when both vehicles travel in the same direction. The models were compared to the recorded channel in terms of the BER statistics of the simulated DSRC standard. The quality of the match between synthesized and recorded channel BER statistics was found to be sensitive to the type of modulation (fixed or adaptive), the frame length, and the length of the interval over which BER was calculated. The best match was for short (64 symbol) interval lengths, and when the modulation and frame length were the same for the design and for the evaluation of the models. The partitions based on BER performed only slightly better than partitions based on number of delays. This indicates at least a weak connection

between the BER approach taken in this paper and the “path lifetime” approach taken by other authors seeking to model the time evolution of large scale random fluctuations of the wireless channel. Perhaps a more direct “path lifetime” approach to this V2V channel might bring the longer-term average BER statistics into better agreement by increasing the burstiness of the V2V model.

Frequency alignment of the spectra prior to averaging was a major factor in the matching of BER statistics. However, even with alignment, spectrum averaging still had two significant drawbacks: broader spectra and higher BERs than the recorded channel for the lowest BER partitions, and reduction of the K factor in the early taps. More work is required to determine how best to produce models with accurate tap K factors, especially for programming RF channel emulators.

Acknowledgements

The authors gratefully acknowledge the support for this work provided by the National Science Foundation under Grant No. CCR-0121565, and by ARINC, Inc., Contract No. DTFH6199-C-00018.

References

1. C.R. Dow, P.J. Lin, S.C. Chen, J.H. Lin, and S.F. Hwang, “A Study of Recent Research Trends and Experimental Guidelines in Mobile Ad-hoc Network”, in *Proc. of Advanced Information Networking and Applications 19th International Conference*, Vol. 1, pp. 72–77, March 2005.
2. R. Ramanathan, J. Redi, C. Santivanez, D. Wiggins, and S. Polit, “Ad Hoc Networking with Directional Antennas: A Complete System Solution”, in *IEEE Journal on Selected Areas in Communications*, Vol. 23, No. 3, pp. 496–506, March 2005.
3. Heo Nojeong and P.K. Varshney, “Energy-Efficient Deployment of Intelligent Mobile Sensor Networks”, *IEEE Transactions on Systems, Man and Cybernetics*, Vol. 35, No. 1, pp. 78–92, January 2005.
4. H. Gharavi and K. Ban, “Multihop Sensor Network Design for Wide-Band Communications”, *IEEE Proceedings*, Vol. 91, No. 8, pp. 1221–1234, August 2003.
5. R.U. Nabar, H. Bölcskei, and F.W. Kneubühler, “Fading Relay Channels: Performance Limits and Space-Time Signal Design”, *IEEE Journal on Selected Areas in Communications*, Vol. 22, No. 6, pp. 1099–1109, August 2004.
6. Zhu Jing and S. Roy, “MAC for Dedicated Short Range Communications in Intelligent Transport System”, in *IEEE Communications Magazine*, Vol. 41, No. 12, pp. 60–67, December 2003.
7. ASTM E 2213-03, “Standard Specification for Telecommunications and Information Exchange between Roadside and Vehicle Systems– 5.9 GHz Band Dedicated Short Range Communications (DSRC) Medium Access Control (MAC) and Physical Layer (PHY) Specifications”, *ASTM International*, www.astm.org.
8. C.-C. Chong, C.-M. Tan, D.I. Laurenson, S. McLaughlin, M.A. Beach, and A.R. Nix, “A Novel Wideband Dynamic Directional Indoor Channel Model Based on a Markov Process”, in *IEEE Transactions on Wireless Communications*, Vol. 4, No. 4, pp. 1539–1552, July 2005.
9. J. O. Nielsen, V. Afanassiev, and J.B. Andersen, “A Dynamic Model for the Indoor Channel”, in *KAP Journal of Wireless Personal Communications*, Vol. 19, pp. 91–120, 2001.
10. M. Newton, D. Kitchener, and M.S. Smith, “Wideband Channel Dynamics (Measurement and Simulation)”, in *Proc. of 11th International Antennas and Propagation Conf.*, pp. 428–431, April 2001.
11. T. Zwick, C. Fischer, and W. Wiesbeck, “A Stochastic Multipath Channel Model Including Path Directions for indoor Environments”, in *IEEE Journal on Selected Areas in Communications*, Vol. 20, No. 6, pp. 1178–1192, August 2002.

12. W. Mohr, "Modeling of Wideband Mobile Radio Channels Based on Propagation Measurements", in *Proc. 16th Int. Symp. Personal, Indoor, Mobile Radio Communications*, Vol. 2, pp. 397–401, 1995.
13. C.S. Patel, G.L. Stüber, and T.G. Pratt, "Simulation of Rayleigh Faded Mobile-to-Mobile Communication Channels", in *Proc. of IEEE Vehicular Technology Conf.*, Vol. 1, pp. 163–167, October 2003.
14. F. Vatalaro and A. Forcella, "Doppler Spectrum in Mobile-to-Mobile Communications in the Presence of Three-Dimensional Multipath Scattering", *IEEE Trans. on Vehic. Tech.*, Vol. 46, No. 1, pp. 213–219, 1997.
15. J. Maurer, T. Fügenm, and W. Wiesbeck, "Narrow-Band Measurement and Analysis of the Inter-Vehicle Transmission Channel at 5.2 GHz", in *Proc. of IEEE Vehicular Technology Conf.*, Vol. 3, pp. 1274–1278, 2002.
16. X. Zhao, J. Kivinen, P. Vainikainen, and K. Skog, "Characterization of Doppler Spectra for Mobile Communications at 5.3 GHz", *IEEE Trans. Vehicular Technology*, Vol. 52, No. 1, pp. 14–23, 2003.
17. G. Acosta, K. Tokuda, and M. A. Ingram, "Measured Joint Doppler-Delay Power Profiles for Vehicle-to-Vehicle Communications at 2.4 GHz", in *Proc. of IEEE Global Telecom. Conf.*, Vol. 6, pp. 3813–3817, 2004.
18. J.D. Parsons, D.A. Demery, and A.M.D. Turkmani, "Sounding Techniques for Wideband Mobile Radio Channels: A Review", *IEE Proceedings*, Vol. 138, no. 5, pp. 437–446, 1991.
19. W.C.Y. Lee, "Estimate of Local Average Power of Mobile Radio Signal", in *IEEE Transactions on Vehicular Technology*, Vol. 34, No. 1, pp. 22–27, February 1985.
20. A. Abdi, C. Tepedelenlioglu, M. Kaveh, and G. Giannakis, "On the Estimation of the K Parameter for the Rice Fading Distribution", in *IEEE Communications Letters*, Vol. 5, No. 3, pp. 92–94, March 2001.
21. L.J. Greenstein, D.G. Michelson, and V. Erceg, "Moment-Method Estimation of the Ricean K -Factor", in *IEEE Communications Letters*, Vol. 3, No. 6, pp. 175–176, June 1999.
22. M.C. Jeruchim, P. Balaban, and K.S. Shanmugan, *Simulation of Communication Systems: Modeling, Methodology, and Techniques*, Second Edition, Kluwer Academic Press, Boston 2000.
23. M.H. Hsieh and C.H. Wei, "Channel Estimation for OFDM Systems Based on Comb-Type Pilot Arrangement in Frequency Selective Channels", in *IEEE Transactions on Consumer Electronics*, Vol. 44, No. 1, pp. 217–225, February 1998.



Guillermo Acosta was born in Mexico City, Mexico, in 1962. He is a Ph.D. Candidate and a graduate research assistant in the School of Electrical and Computer Engineering at the Georgia Institute of Technology, in Atlanta, Georgia. He obtained his Bachelor of Engineering with Honors and Master of Engineering, both in Electrical Engineering, from Stevens Institute of Technology, Hoboken, New Jersey, in 1985 and 1987, respectively. He also obtained a Master of Business Administration with Honors from the Instituto Tecnológico Autónomo de México (ITAM), Mexico City, Mexico, in 1996. Mr. Acosta has held technical and managerial positions in the recording, radio, and TV industries and in the Communications Ministry of Mexico. He has been an adjunct instructor in Electrical Engineering in the Instituto Tecnológico y Estudios Superiores de Monterrey Campus Estado de México (ITESM-CEM) and the Universidad Iberoamericana. He is member of the IEEE, INCE, Tau Beta Pi, and Eta Kappa Nu.



Mary Ann Ingram received the B.E.E. and Ph.D. degrees from the Georgia Institute of Technology, in Atlanta, Georgia, in 1983 and 1989, respectively. From 1983 to 1986, she was a Research Engineer with the Georgia Tech Research Institute in Atlanta, performing studies on radar electronic countermeasure (ECM) systems. In 1986, she became a graduate research assistant with the School of Electrical and Computer Engineering at the Georgia Institute of Technology, where in 1989, she became a Faculty Member and is currently Professor. Her early research areas were optical communications and radar systems. In 1997, she established the Smart Antenna Research Laboratory (SARL), which emphasizes the application of multiple antennas to wireless communication systems. The SARL performs system analysis and design, channel measurement, and prototyping, relating to a wide range of wireless applications, including wireless local area network (WLAN) and satellite communications, with focus on the lower layers of communication networks. Dr. Ingram is a Senior Member of the IEEE.